Current transport mechanisms in plasma-enhanced atomic layer deposited AlN thin films

Halit Altuntas, Cagla Ozgit-Akgun, Inci Donmez, and Necmi Biyikli

Citation: Journal of Applied Physics **117**, 155101 (2015);
View online: https://doi.org/10.1063/1.4917567
View Table of Contents: http://aip.scitation.org/toc/jap/117/15
Published by the American Institute of Physics

JOURNAL OF APPLIED PHYSICS 117, 155101 (2015)

Current transport mechanisms in plasma-enhanced atomic layer deposited AlN thin films

Halit Altuntas,[1,a)] Cagla Ozgit-Akgun,[2,3] Inci Donmez,[2,3] and Necmi Biyikli[2,3,a)]
[1]*Faculty of Science, Department of Physics, Cankiri Karatekin University, Cankiri 18100, Turkey*
[2]*National Nanotechnology Research Center (UNAM), Bilkent University, Bilkent, Ankara 06800, Turkey*
[3]*Institute of Materials Science and Nanotechnology, Bilkent University, Bilkent, Ankara 06800, Turkey*

(Received 4 February 2015; accepted 2 April 2015; published online 15 April 2015)

Here, we report on the current transport mechanisms in AlN thin films deposited at a low temperature (i.e., 200 °C) on *p*-type Si substrates by plasma-enhanced atomic layer deposition. Structural characterization of the deposited AlN was carried out using grazing-incidence X-ray diffraction, revealing polycrystalline films with a wurtzite (hexagonal) structure. Al/AlN/ *p*-Si metal-insulator-semiconductor (MIS) capacitor structures were fabricated and investigated under negative bias by performing current-voltage measurements. As a function of the applied electric field, different types of current transport mechanisms were observed; i.e., ohmic conduction (15.2–21.5 MV/m), Schottky emission (23.6–39.5 MV/m), Frenkel-Poole emission (63.8–211.8 MV/m), trap-assisted tunneling (226–280 MV/m), and Fowler-Nordheim tunneling (290–447 MV/m). Electrical properties of the insulating AlN layer and the fabricated Al/AlN/*p*-Si MIS capacitor structure such as dielectric constant, flat-band voltage, effective charge density, and threshold voltage were also determined from the capacitance-voltage measurements. © *2015 AIP Publishing LLC*.
[http://dx.doi.org/10.1063/1.4917567]

I. INTRODUCTION

Binary and ternary III-nitride semiconductors are appealing materials for the micro- and opto-electronics industries due to their potential device applications.[1–4] Among this group of materials, aluminum nitride (AlN) attracted lots of attention due to its direct and wide band gap of 6.2 eV, excellent thermal conductivity, good piezoelectric properties, good chemical and thermal stability, and high acoustic velocity. Moreover, AlN has a high dielectric constant, which makes it a potential insulating material for metal-insulator-semiconductor (MIS) devices.[5] AlN thin films have been deposited by various methods including molecular beam epitaxy,[6] metal-organic chemical vapor deposition (MOCVD),[7] ion beam deposition,[8] magnetron sputtering,[9] pulsed laser deposition,[10] and plasma-enhanced chemical vapor deposition.[11] Although MOCVD-grown AlN thin films are being widely used in today's semiconductor technology, MOCVD growth inherently takes place at high temperatures, which is incompatible with device applications requiring the use of temperature sensitive device layers and flexible substrates. When considered from this point of view, atomic layer deposition (ALD) is an alternative low-temperature thin film deposition method, which consists of sequential and non-overlapping injections of two or more gas-phase precursors with a well-defined periodicity. The ALD technique is inherently self-limiting; once a monomolecular layer of a precursor is chemisorbed on the substrate surface, the gas-solid reaction stops since the precursor molecules of the same kind do not react with each other. The critical advantages of ALD over other deposition techniques can therefore be listed as the deposition of highly conformal, uniform, and smooth thin films with sub-nanometer thickness control, deposition at low temperatures, and low residual stress in the deposited layers.[12,13] ALD temperatures can also be further decreased by the enhancement of surface reactions via an additional energy source, such as plasma. Plasma-enhanced ALD (PEALD) is a widely used technique, in which plasma source creates highly reactive radicals that contribute to chemical reactions occurring at the substrate surface. When compared to conventional thermal ALD, PEALD provides a wider range of materials deposition capability at relatively low substrate temperatures.

In the previous reports, we investigated the self-limiting growth of crystalline AlN thin films at low temperatures by PEALD using trimethylaluminum (TMA) and ammonia (NH_3) as the aluminum and nitrogen precursors, respectively.[14,15] Here, we present the room-temperature electrical conduction properties of these polycrystalline wurtzite AlN thin films, along with some other electrical properties, as determined from the current-voltage (*I-V*) and high-frequency (1 MHz) capacitance-voltage (*C-V*) measurements of Al/AlN/*p*-Si MIS structures.

II. EXPERIMENTAL METHOD

MIS capacitor structures with AlN as the insulating layer were fabricated on 25 mm × 40 mm *p*-type Si (100) substrates ($\rho = 20$–$40\ \Omega$ cm) using class 100 and 1000 cleanroom facilities. Solvent-cleaned substrates were subjected to piranha etch (H_2SO_4:$H_2O_2 = 4$:1) for 5–10 min, which was followed by the native oxide removal in dilute hydrofluoric acid solution (HF, 2 vol. %) for 2–3 min. Back ohmic contacts were formed by thermal evaporation and subsequent rapid thermal annealing. First, ~80 nm thick Al was deposited to the back side of each wafer using VAKSIS Thermal Evaporation System (PVD Vapor 3S Thermal), while the top

a)Authors to whom correspondence should be addressed. Electronic addresses: altunhalit@gmail.com and biyikli@unam.bilkent.edu.tr.

sides were protected with a layer of photoresist. After stripping the photoresist layers and washing the samples alternately with acetone, methanol, isopropanol, and deionized (DI) water, and then drying with N_2, samples were annealed in ATV-Unitherm (RTA SRO-704) rapid thermal annealing system at 450 °C for 2 min under 100 sccm N_2 flow. Ramping rate was 15 °C/min. Si (100) substrates with back ohmic contacts and solvent-cleaned bare Si (100) substrates (for characterization purposes) were then loaded into a Fiji F200-LL ALD reactor (Cambridge Nanotech Inc.) immediately after they were dipped into dilute HF solution, rinsed with DI water and dried with N_2. 175 cycles AlN were deposited on these substrates at 200 °C, where one PEALD cycle consisted of: 0.1 s TMA pulse/10 s Ar purge/40 s, 50 sccm, 300 W NH_3 plasma/10 s Ar purge. During the deposition, TMA and NH_3 were carried from separate lines using 60 and 200 sccm Ar, respectively. Base pressure was 30 Pa. Top contacts were then formed by thermal evaporation (~80 nm thick Al) and photolithography. Al and AlN layers were patterned simultaneously to obtain 250 μm × 250 μm MIS devices during the development of AZ 5214 E photoresist with AZ 400 K developer (AZ 400 K:H_2O = 1:4).

Capacitance-voltage (*C-V*) and current-voltage (*I-V*) characteristics of the fabricated MIS capacitor structures were measured under dark using a semiconductor parameter analyzer (Keithley 4200-SCS), which is connected to a probe station (Cascade Microtech PM-5). *C-V* curves were obtained at a frequency of 1 MHz. AlN films deposited on solvent-cleaned and HF-dipped bare Si (100) substrates were characterized by spectroscopic ellipsometry, X-ray photoelectron spectroscopy (XPS), X-ray reflectivity (XRR), and grazing incidence X-ray diffraction (GIXRD). Ellipsometric spectra of the films were recorded in the wavelength range of 300–850 nm at three angles of incidence (65°, 70°, and 75°) using a variable angle spectroscopic ellipsometer (J.A. Woollam). Optical constants and film thicknesses were extracted using the Cauchy dispersion function using a two-layer model; i.e., Cauchy/Si (0.5 mm). Chemical compositions of the films were determined by XPS using Thermo Scientific K-Alpha spectrometer with a monochromatized Al Kα X-ray source. The pass energy, step size, and spot size were 30 eV, 0.1 eV, and 400 mm, respectively. Etching of the samples was carried out *in situ* with a beam of Ar ions having an acceleration voltage of 1 kV. XRR and GIXRD measurements were performed in a PANalytical X'Pert PRO MRD diffractometer using Cu Kα radiation.

III. RESULTS AND DISCUSSION

A. Film structure and capacitance-voltage (C-V) characteristics

GIXRD pattern of the AlN thin film deposited at 200 °C on a Si (100) substrate by the application of 175 PEALD cycles is given in Fig. 1. On the pattern, (100), (002), (101), (102), (110), (103), and (112) reflections of the hexagonal phase were observed (ICDD reference code: 00-025-1133), indicating a polycrystalline AlN film with wurtzite (hexagonal) structure. The refractive index (*n*) of the PEALD-grown AlN thin film was measured within the wavelength range of

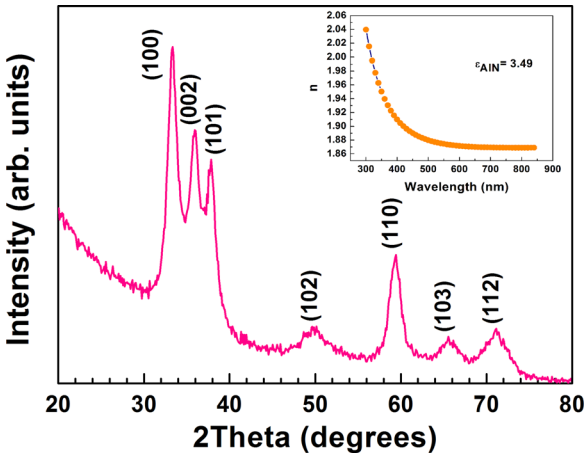

FIG. 1. GIXRD pattern of the AlN thin film deposited at 200 °C on Si (100) substrate. Film is polycrystalline with a hexagonal wurtzite structure. Inset shows the spectral refractive index (*n*) of the deposited AlN thin film.

300–850 nm by spectroscopic ellipsometry. As can be seen from the inset of Fig. 1, refractive index decreases from 2.04 to 1.87 as the wavelength increases from 300 nm to 850 nm. As known, *n* value depends on film crystallinity; the *n* values that were reported in the literature for polycrystalline AlN films[16] are in good agreement with the present data, which again confirms the polycrystalline nature of the deposited films. The optical dielectric constant (κ_{op}) is equal to the square of the refractive index, which was already obtained by spectroscopic ellipsometry (i.e., $\kappa_{op} = n^2$). *n* value of the deposited AlN was measured to be 1.87 at 633 nm, resulting in a κ_{op} of 3.49.

The typical high-frequency (1 MHz) *C-V* characteristics of Al/AlN/*p*-Si MIS capacitors are presented in Fig. 2. The *C-V* characteristics exhibited a negative flat-band voltage shift, which is associated with the presence of trapped positive charges as the nitride equivalent of fixed oxide charges in the dielectric films or AlN/Si interface. Al/AlN/*p*-Si MIS capacitors also showed *C-V* hysteresis behavior (see inset of Fig. 2) due to the presence of mobile charges inside the AlN film and trapped charges at the interface. The *C-V* curve looped counterclockwise when swept from accumulation to

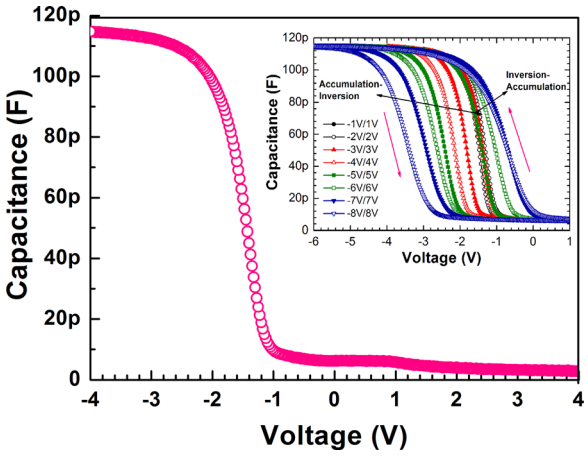

FIG. 2. High-frequency *C-V* curve of an Al/AlN/*p*-Si MIS device fabricated using PEALD-grown AlN insulating layer. Inset shows the hysteresis behaviors of the fabricated MIS capacitors.

inversion, implying that the hysteresis behavior is mainly due to hole injection from Si into the dielectric AlN layer since flat-band voltage shifts in the accumulation-inversion branches are larger than those in the inversion-accumulation branches. The magnitude of the hysteresis width (i.e., memory window) was found to be dependent on the voltage sweeping range. In general, the memory window increases with gate bias, indicating the injection of increased number of charges.[17]

The effective charges—depending on their type—shift the *C-V* curve to either left or right. The effective charge density (N_{eff}) can be calculated using the flat-band voltage (V_{FB}) that is graphically determined from the *C-V* curves. The N_{eff} and flat-band voltage are related to each other by

$$N_{eff} = \frac{C_i(\phi_{ms} - V_{FB})}{qA}, \tag{1}$$

where ϕ_{ms} is the difference between metal (Al) and semiconductor (Si) work functions, q is the electronic charge, C_i is the capacitance of the insulator under strong accumulation mode, and A is the area of the capacitor, which was calculated to be 5.93×10^{-4} cm^2 for the present case.

Electrical and optical properties of the materials are influenced by the dielectric constant (ε_r), which can be obtained by substituting the value of C_i under strong accumulation mode into the following equation:

$$C_i = \frac{\varepsilon_r \varepsilon_o A}{t_d}, \tag{2}$$

where ε_o is the permittivity of vacuum and t_d is the thickness of the dielectric layer (i.e., ~14.4 nm). The dielectric constant was therefore estimated to be 3.15 for the deposited AlN film. In the following text, this dielectric constant will be mentioned as the *static dielectric constant*.

In order to determine the flat-band voltage, flat-band capacitance (C_{FB}) method was used. The *p*-type Si surface at the flat-band condition is given by

$$C_{FBS} = \frac{\varepsilon_{Si}\varepsilon_o}{\lambda}, \tag{3}$$

where ε_{Si} is the dielectric constant of Si (i.e., 11.8) and λ is the Debye length of *p*-type Si, which is expressed as

$$\lambda = \left(\frac{\varepsilon_{Si}\varepsilon_o kT}{q^2 N_A}\right)^{1/2}, \tag{4}$$

where k is the Boltzmann constant, T is the absolute temperature, and N_A is the doping concentration of *p*-type Si. The N_A values were calculated from the slopes of $1/C^2$–V graphs and found to be 1.13×10^{15} cm^{-3}. Following the calculation of C_{FBS}, the flat-band capacitance C_{FB} can be obtained using the series capacitance relationship

$$C_{FB} = \frac{C_o C_{FBS}}{C_o + C_{FBS}}. \tag{5}$$

The flat-band voltage (V_{FB}) is the voltage value corresponding to C_{FB} on the high-frequency *C-V* curves, which was graphically determined to be −1.35 V. By substituting this value in Eq. (1), N_{eff} was found as 6.4×10^{11} cm^{-2} for the deposited films. Calculated electrical parameters of PEALD-grown AlN thin films are summarized in Table I. Effective charge density (N_{eff}) values on the order of 10^{12} cm^{-2} and 10^{13} cm^{-2} were reported for AlN thin films deposited by sequential injection of TMA and NH_3 under UV radiation,[18] radio frequency (RF) magnetron sputtering,[19] reactive sputtering,[20] d.c. magnetron sputtering,[21] and RF magnetron sputtering.[22] The value reported herein (i.e., 6.4×10^{11} cm^{-2}) is therefore better than those reported in the literature for AlN thin films deposited using various methods and suggests that AlN thin films with low effective charge densities can be deposited successfully using low-temperature PEALD.

Another important electrical parameter of a capacitor is the threshold onset voltage (V_{th}). This parameter can be calculated for strong inversion of the MIS device (*p*-type substrate) according to the following relation:[23]

$$V_{th} = V_{FB} + 2\phi_b + \frac{(4q\varepsilon_{Si}\varepsilon_o N_A|\phi_b|)^{1/2}}{\varepsilon_{ox}\varepsilon_o / t_{ox}}, \tag{6}$$

where $\phi_b = (k_B T/q)\ln(N_A/n_i)$ and n_i is the intrinsic carrier concentration of Si at room temperature (i.e., 1.45×10^{10} cm^{-3}). Substituting these parameters into Eq. (6) yields the V_{th} value as −0.67 V for Al/AlN/*p*-Si MIS capacitors investigated in this study.

B. Current transport mechanisms under negative bias

Electrical conduction behaviors of the AlN capacitors were investigated under d.c. bias. Measured current densities (J) of the Al/AlN/*p*-Si capacitors under negative gate bias (NGB) are given in Fig. 3. It is well-known that many conduction mechanisms can be observed for dielectric materials depending on the magnitude of applied electric field. For AlN thin films deposited using PEALD, we observed five different regions on the *J-V* plot, which represent different transport mechanisms under NGB. Each of these regions will be explained in detail in the following paragraphs along with the corresponding current transport mechanisms.

Fig. 4 shows the ln (J) vs. ln (E) graph for Al/AlN/*p*-Si capacitors under NGB, where E is the electric field, values of which were obtained from the formula $E = (V - V_{FB})/t_{AlN}$. As seen from this figure, plot is initially linear at the low electric field region (i.e., 15.2–21.5 MV/m). In this region, current density is proportional to the electric field, and the slope of the plot is about 1. This behavior indicates that the

TABLE I. Electrical parameters of the PEALD-grown AlN thin films as extracted from high-frequency *C-V* curves.

λ-Debye length (cm)	C_{FBS} (F)	C_i (F)	C_{FB} (F)	V_{FB} (V)	ϕ_{ms} (eV)	ε_r	N_{eff} (cm^{-2})	V_{th} (V)
1.2×10^{-5}	5.08×10^{-11}	1.15×10^{-10}	3.52×10^{-11}	−1.35	−0.82	3.15	6.4×10^{11}	−0.67

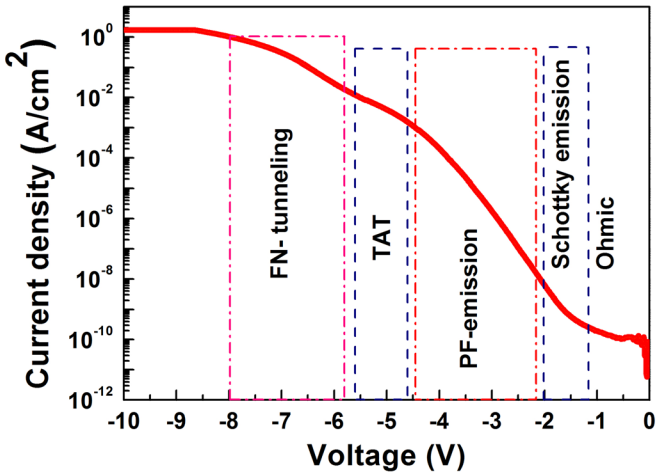

FIG. 3. Current density-voltage characteristics of the Al/AlN/*p*-Si MIS capacitor structures.

current transport mechanism in this E range is *Ohmic conduction*.

The *Schottky emission (SE)* mechanism is described as

$$J \propto A^{*}T^{2}\exp\left[\frac{-q\left(\phi_B-\sqrt{qE/4\pi\varepsilon_r\varepsilon_o}\right)}{k_BT}\right], \qquad (7)$$

where J is the current density, E is the electric field, A^{*} is the effective Richardson constant, ϕ_B is the barrier height, ε_r is the dielectric constant, q is the electronic charge, and k is Boltzmann constant. If SE applies, then the ε_r value can be calculated from the ln (J) vs. $E^{1/2}$ plot using Eq. (7). From the ln (J) vs. $E^{1/2}$ graph (see Fig. 5), ϕ_B and ε_r were calculated to be 1.02 eV and 3.17, respectively. The calculated ε_r value is in good agreement with the values obtained from high frequency C-V measurement (i.e., 3.15) and spectroscopic ellipsometry ($\kappa_{op}=3.49$). These results indicate that the conduction mechanism in the E range of 23.6–39.5 MV/m is SE.

Current conduction in PEALD-grown AlN films is governed by a different transport mechanism, *Frenkel-Poole emission (FP)*, under the substrate hole injection and at relatively high electric fields (i.e., 63.8–211.8 MV/m).

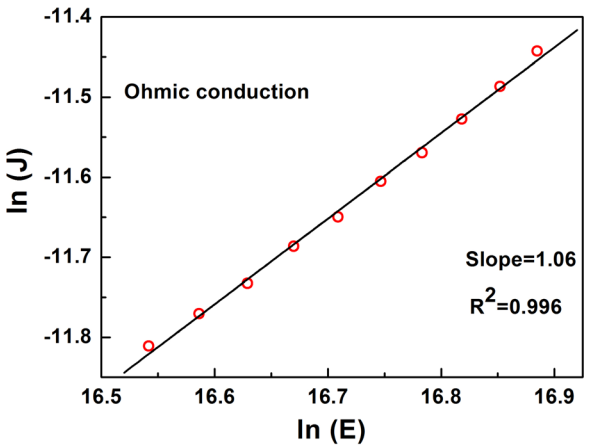

FIG. 4. ln (J) vs. ln (E) plot of the Al/AlN/*p*-Si MIS capacitor structures.

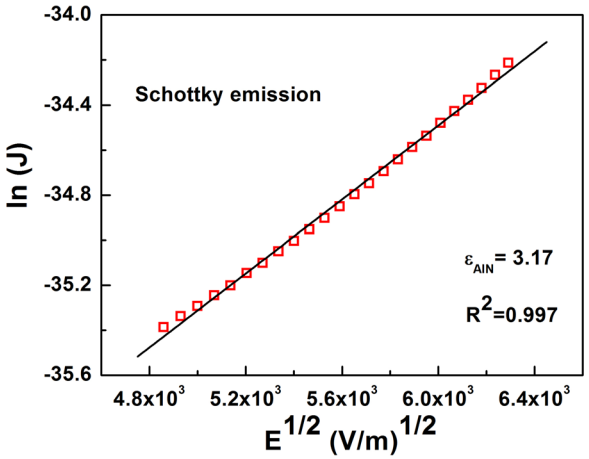

FIG. 5. Schottky emission model fitted for the determination of conduction mechanisms in Al/AlN/*p*-Si MIS capacitor structures.

FP is the field-assisted thermal de-trapping of a carrier from bulk dielectric into conduction band; therefore, it is a "bulk-limited" conduction process. Current density due to FP is given as

$$J \propto E\exp\left[\frac{-q\left(\phi_t-\sqrt{qE/\pi\varepsilon_r\varepsilon_o}\right)}{k_BT}\right], \qquad (8)$$

where ϕ_t is the trap energy level; i.e., the energy level of the electrically active defect states within the band gap of a dielectric material. According to Eq. (8), the slope of the ln (J/E) vs. $E^{1/2}$ plot provides an estimate for the dielectric constant. The plot is very well fitted ($R^2=0.999$) with the FP mechanism as shown in Fig. 6, and ϕ_t and ε_r were calculated as 0.98 eV and 3.82, respectively. This ε_r value agrees well with the optical and static dielectric constants, thus confirming the presence of FP conduction mechanism in the 63.8–211.8 MV/m range. The ϕ_t value calculated in this study (i.e., 0.98 eV) is higher than those reported by Engelmark *et al.*[20] and Hassine *et al.*[24] According to Wu *et al.*,[25] dangling bonds in the aluminum tend to give rise to ~1 eV in ϕ_t for metal-rich AlN films. XPS analysis of the PEALD-grown film revealed Al/N ratios of 1.5 and 1.03 at the film surface and bulk, respectively, indicating slightly Al-rich AlN thin films. The higher value of the ϕ_t as

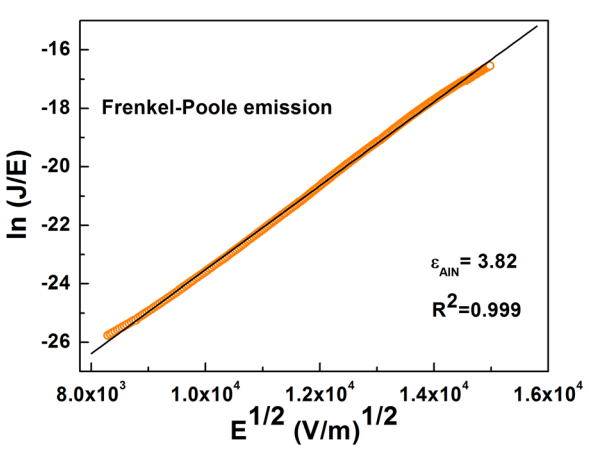

FIG. 6. Frenkel-Poole plot of the Al/AlN/*p*-Si MIS capacitor structures.

compared to those reported in the literature might therefore be attributed to the dangling bonds of excess aluminum in deposited films.

Fig. 7 is the ln (J) vs. $1/E$ under the substrate injection condition. At moderately high electric fields (i.e., 226–280 MV/m), a perfect linear variation ($R^2 = 1$) of ln (J) vs. $1/E$ was observed, which points out that the conduction mechanism within this range is *trap assisted tunneling (TAT)*. The current due to TAT mechanism is given by the following equation:

$$J_{TAT} \propto \exp\left\{\frac{-8\pi\sqrt{2qm_{AlN}}}{3hE}\phi_t^{3/2}\right\}, \quad (9)$$

where ϕ_t is the energy level of the electronic defect states, which was graphically obtained from the plot of ln (J) vs. $1/E$ as 0.6 eV. The obtained ϕ_t value is equal to that of a nitrogen vacancy in crystalline AlN as predicted by Jenkins and Dow.[26] Moreover, Ligatchev *et al.*[27] reported defect state energy levels of 0.47–0.62 eV and 0.73–0.80 eV for nitrogen vacancies in AlN deposited on silicon. Thus, the obtained energy level of electronic defect states is related to the nitrogen vacancies, which are responsible for electron conduction in AlN.

Finally, for the 290–447 MV/m electric field region in the J-V plot, the current density was fitted by the *Fowler-Nordheim (FN) tunneling* mechanism. The FN tunneling current density is given as

$$J_{FN} \propto E^2 \exp\left\{\frac{-8\pi\sqrt{2qm_{AlN}}}{3hE}\phi_b^{3/2}\right\}, \quad (10)$$

where ϕ_b is the barrier height at the emitting interface. Fig. 8 is the plot of ln (J/E^2) vs. $1/E$, which shows a linear relationship for the indicated electric field range. From the slope of this plot, ϕ_b was calculated to be 0.84 eV. However, the derived barrier height is much lower than 3.48 eV at the Al/AlN interface. Therefore, an electron transferring from metal gate to the dielectric may be emitted from electronic defect states at the metal/dielectric interface via FN tunneling.

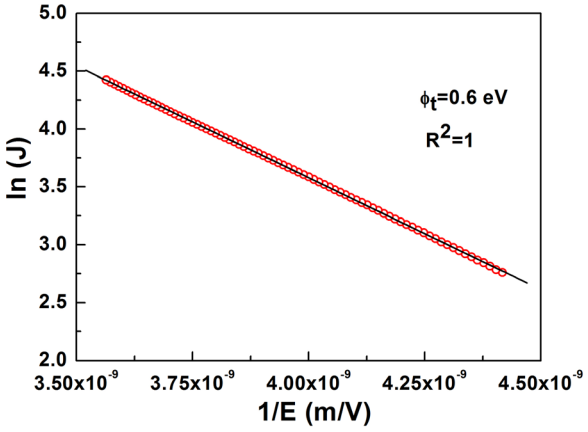

FIG. 7. ln (J) vs. $1/E$ plot (i.e., the TAT plot).

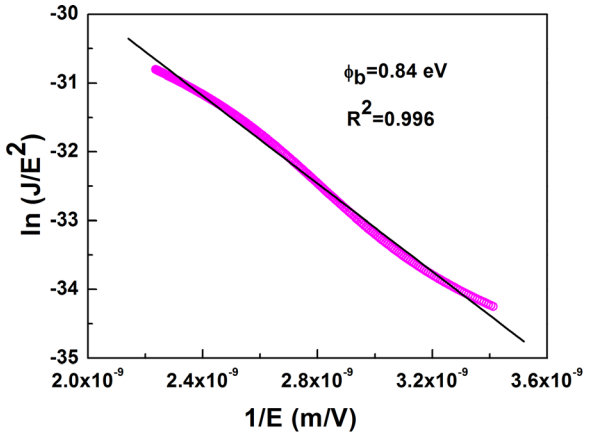

FIG. 8. ln (J/E^2) vs. $1/E$ plot (i.e., the FN tunneling plot).

IV. CONCLUSION

In this work, polycrystalline wurtzite AlN thin films were deposited on p-Si substrates at 200 °C by PEALD, using TMA and NH_3 as the aluminum and nitrogen precursors, respectively. Electric-field dependent current transport mechanisms of the fabricated Al/AlN/p-Si MIS structures were investigated. Within the low-field regime, the conduction mechanisms were determined as ohmic conduction and Schottky emission (15.2–21.5 MV/m and 23.6–39.5 MV/m, respectively), whereas for higher electric field, the conduction mechanisms were found to be Frenkel-Poole emission (63.8–211.8 MV/m), trap assisted tunneling (226–280 MV/m), and Fowler-Nordheim tunneling (290–447 MV/m). The calculated energy levels of the electronic defect states are attributed to the dangling bonds present as a result of excess aluminum, and nitrogen vacancies in the polycrystalline AlN. Furthermore, several critical electrical parameters of the capacitor structures, as well as the insulating layer, such as dielectric constant, flat-band voltage, effective charge density, and threshold voltage were determined using the C-V measurements. The results show that these low-temperature PEALD-grown AlN films have a significant potential for various electronic applications. Recently, we deposited AlN thin films with reduced impurity contents using a novel approach, which relies on the use of a hollow cathode plasma source. Electrical properties of these higher quality PEALD-grown AlN thin films are still under investigation.

ACKNOWLEDGMENTS

This work was performed at UNAM supported by the State Planning Organization (DPT) of Turkey through the National Nanotechnology Research Center Project. N. Biyikli acknowledges Marie Curie International Reintegration Grant (IRG) for funding NEMSmart (PIRG05-GA-2009-249196) project.

[1]H. Oikawa, R. Akiyama, K. Kanazawa, S. Kuroda, I. Harayama, K. Nagashima, D. Sekiba, Y. Ashizawa, A. Tsukamoto, K. Nakagawa, and N. Ota, Thin Solid Films **574**, 110 (2015).
[2]I. Yonenaga, Y. Ohno, T. Yao, and K. Edagawa, J. Cryst. Growth **403**, 72 (2014).
[3]S. Nakamura, Jpn. J. Appl. Phys., Part 2 **35**, L74 (1996).

[4]H. Morkoç, S. Strite, G. B. Gao, M. E. Lin, B. Sverdlov, and M. Burns, J. Appl. Phys. **76**, 1363 (1994).
[5]H. Van Bui, M. D. Nguyen, F. B. Wiggers, A. A. I. Aarnink, M. P. de Joung, and A. Y. Kovalgin, ECS J. Solid State Sci. Technol. **3**, P101 (2014).
[6]M. Placidi, A. Perez-Tomas, J. C. Moreno, E. Frayssinet, F. Semond, A. Constant, P. Godignon, N. Mestres, A. Crespi, and J. Millan, Surf. Sci. **604**, 63 (2010).
[7]C. M. Zetterling, M. Oestling, C. I. Harris, N. Nordell, K. Wongchotigul, and M. G. Spencer, Mater. Sci. Forum **264**, 877 (1998).
[8]C. Men and C. Lin, Mater. Sci. Eng., B **133**, 124 (2006).
[9]M. A. Moreira, I. Doi, J. F. Souza, and J. A. Diniz, Microelectron. Eng. **88**, 802 (2011).
[10]Y. E. Lu, Z. M. Ren, T. C. Chong, B. A. Cheong, S. K. Show, and J. P. Wang, J. Appl. Phys. **87**, 1540 (2000).
[11]G. Sanchez, B. Abdallah, P. Tristant, C. Dublanche-Tixier, M. A. Djouadi, M. P. Besland, P. Y. Jouan, and A. B. Alles, J. Mater. Sci. **44**, 6125 (2009).
[12]H. Kim, J. Vac. Sci. Technol., B **21**, 2231 (2003).
[13]O. M. E. Ylivaara, X. Liu, L. Kilpi, J. Lyytinenn, D. Schneider, M. Laitinen, J. Julin, S. Ali, S. Sintonen, M. Berdova, E. Haimi, T. Sajavaara, H. Ronkaien, H. Lipsanen, J. Koskinen, S.-P. Hannula, and R. L. Puurunen, Thin Solid Films **552**, 124 (2014).
[14]C. Ozgit, I. Donmez, M. Alevli, and N. Biyikli, Thin Solid Films **520**, 2750 (2012).
[15]M. Alevli, C. Ozgit, I. Donmez, and N. Biyikli, Phys. Status Solidi A **209**, 266 (2012).
[16]H. C. Barshilia, B. Deepthi, and K. S. Rajam, Thin Solid Films **516**, 4168 (2008).
[17]W. Guan, S. Long, M. Liu, Z. Li, Y. Hu, and Q. Liu, J. Phys. D: Appl. Phys. **40**, 2754 (2007).
[18]D. Eom, S. Y. No, C. S. Hwang, and H. J. Kim, J. Electrochem. Soc. **153**, C229 (2006).
[19]K. Jang, K. Lee, J. Kim, S. Hwang, J. Lee, S. K. Dhungel, S. Jung, and J. Yi, Mater. Sci. Semicond. Process. **9**, 1137 (2006).
[20]F. Engelmark, J. Westlinder, G. F. Iriarte, I. V. Katardjiev, and J. Olsson, IEEE Trans. Electron Devices **50**, 1214 (2003).
[21]C. Oliviera, M. Massi, S. G. Santos, C. Otani, H. S. Maciel, and R. D. Mansano, Diam. Relat. Mater. **10**, 1317 (2001).
[22]M. S. Lee, S. Wu, S. B. Jhong, K. H. Chen, and K. T. Liu, J. Nanomater. **2014**, 250439.
[23]R. S. Muller and T. I. Kamins, *Device Electronics for Integrated Circuits*, 2nd ed. (Wiley, New York, 1986).
[24]N. B. Hassine, D. Mercier, P. Renaux, G. Parat, S. Basrour, P. Waltz, C. Chappaz, P. Ancey, and S. Blonkowski, J. Appl. Phys. **105**, 044111 (2009).
[25]C. I. Wu and A. Kahn, Appl. Phys. Lett. **74**, 546 (1999).
[26]D. W. Jenkins and J. D. Dow, Phys. Rev. B **39**, 3317 (1989).
[27]V. Ligatchev, Rusli, and Z. Pan, Appl. Phys. Lett. **87**, 242903 (2005).